Electronic Supplementary Material (ESI) for Nanoscale.

Supporting Information

In situ growth of well-aligned Ni-MOF nanosheets on nickel foam for enhanced photocatalytic degradation of typical volatile organic compounds

Xin Ding,[a,#] Hongli Liu,[a,b,#] Jiangyao Chen,[a,b] Meicheng Wen,[a] Guiying Li,[a,b] Taicheng An,[a,*] Huijun Zhao[c,*]

[a] Guangdong Key Laboratory of Environmental Catalysis and Health Risk Control, Guangzhou Key Laboratory Environmental Catalysis and Pollution Control, School of Environmental Science and Engineering, Institute of Environmental Health and Pollution Control, Guangdong University of Technology, Guangzhou 510006, China.

[b] Synergy Innovation Institute of GDUT, Shantou 515041, China.

[c] Centre for Clean Environment and Energy, and Griffith School of Environment, Gold Coast Campus, Griffith University, Queensland, 4222, Australia.

# *Both authors contributed equally to this work and were considered co-first authors.*

*** Corresponding authors.**

Prof. Taicheng An, E-mail: antc99@gdut.edu.cn (T. An),

Prof. Huijun Zhao, E-mail: h.zhao@griffith.edu.au (H. Zhao).

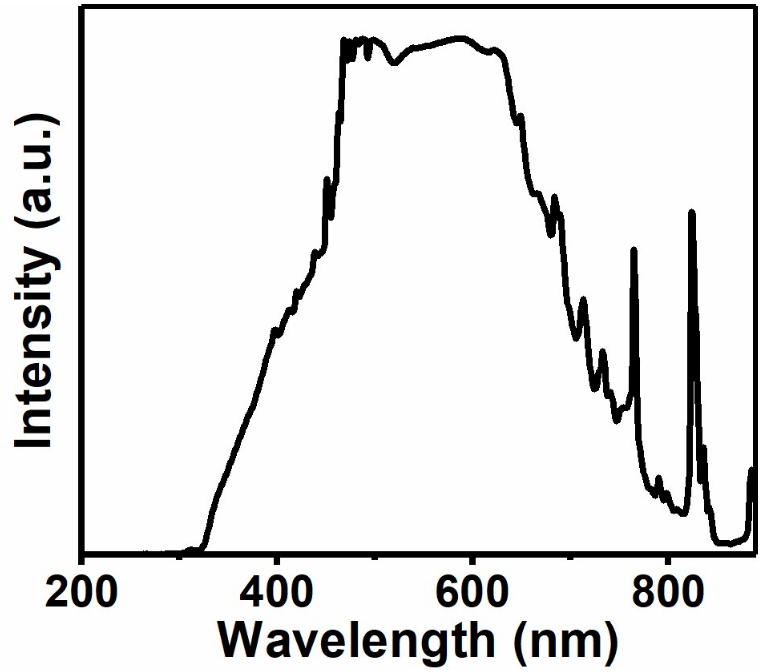

Fig. S1 The measured light spectrum of Xenon lamp.

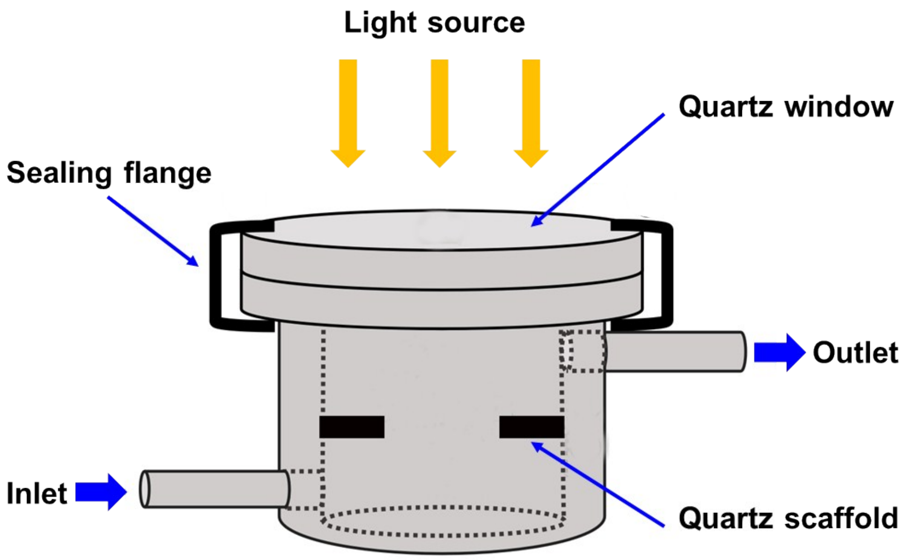

Fig. S2 The diagram of the photocatalytic reactor.

For bare Ni foam and Ni-MOF/NF, they were directly placed onto the quartz scaffold. For powder Ni-MOF, 100 mg of activated Ni-MOF were dispersed onto a mesh with the size of 2 cm × 3 cm and then placed onto the quartz scaffold.

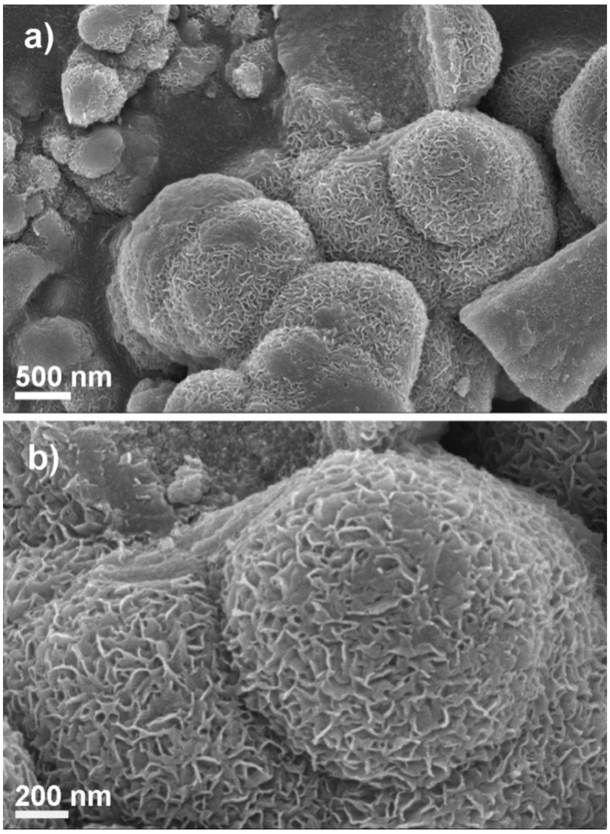

Fig. S3 SEM images of the powder Ni-MOF (a-b).

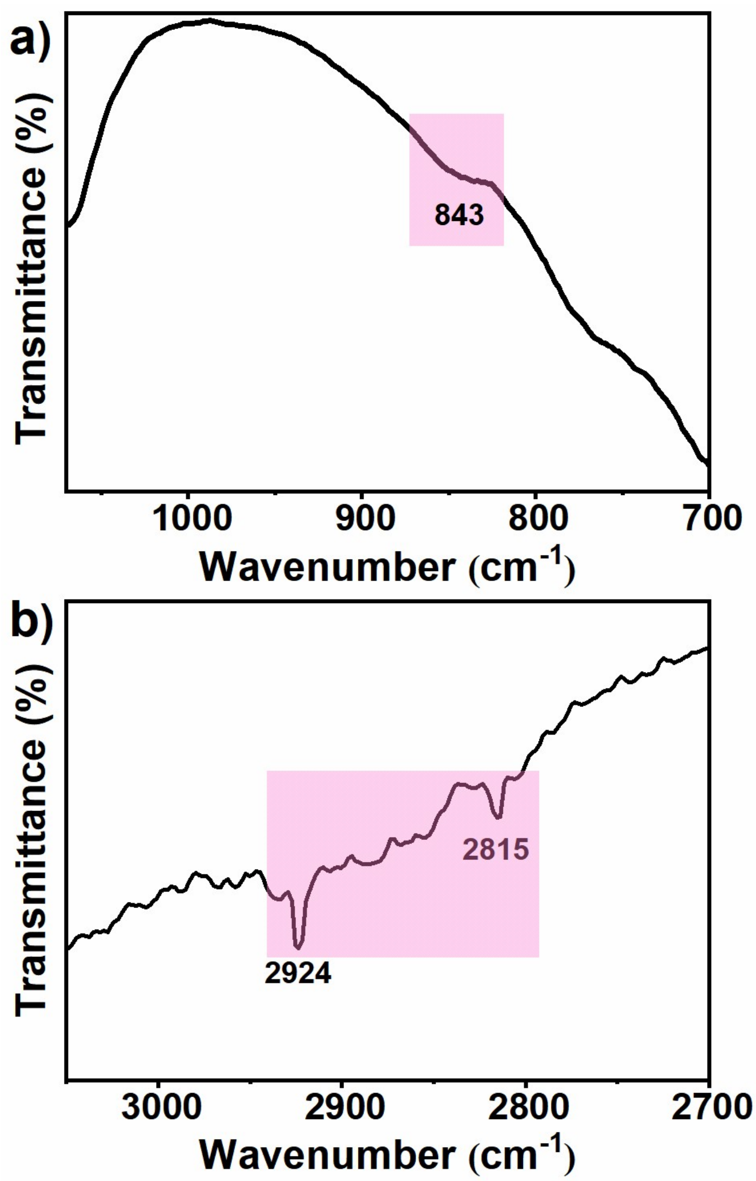

Fig. S4 FT-IR spectrum of Ni-MOF/NF in the ranges of 700-1070 cm^{-1} (a) and 2700-3050 cm^{-1} (b).

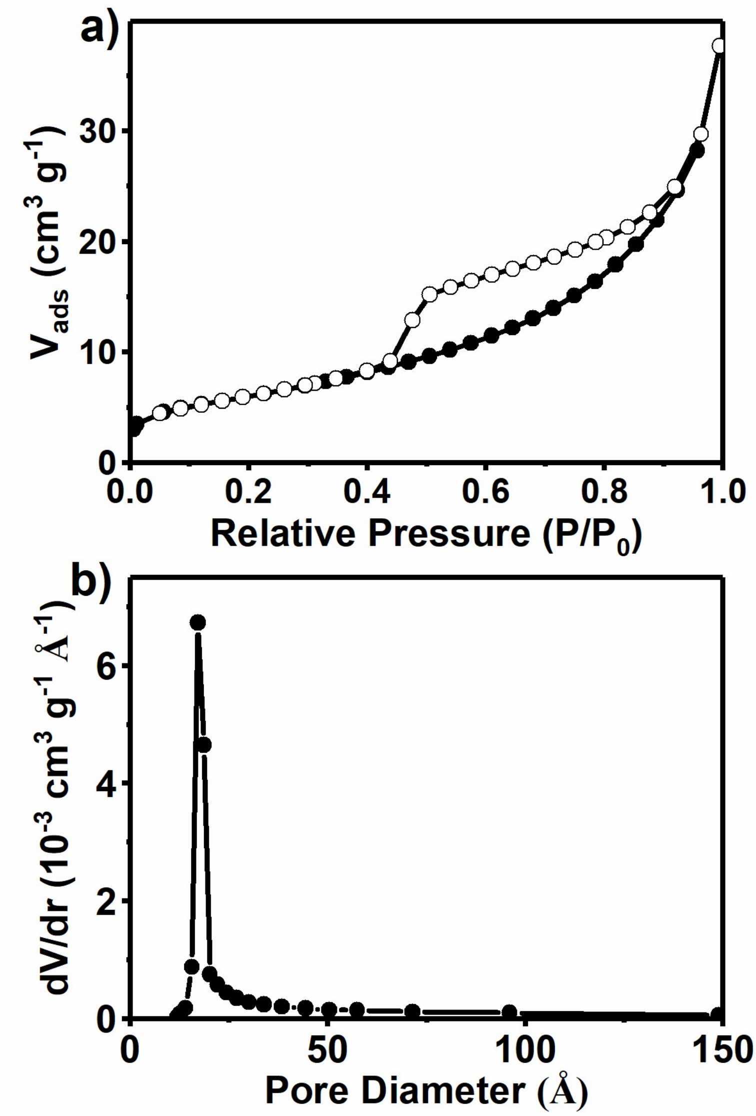

Fig. S5 N_2 adsorption-desorption isotherms (a) and pore-size distribution curves (b) of Ni-MOF.

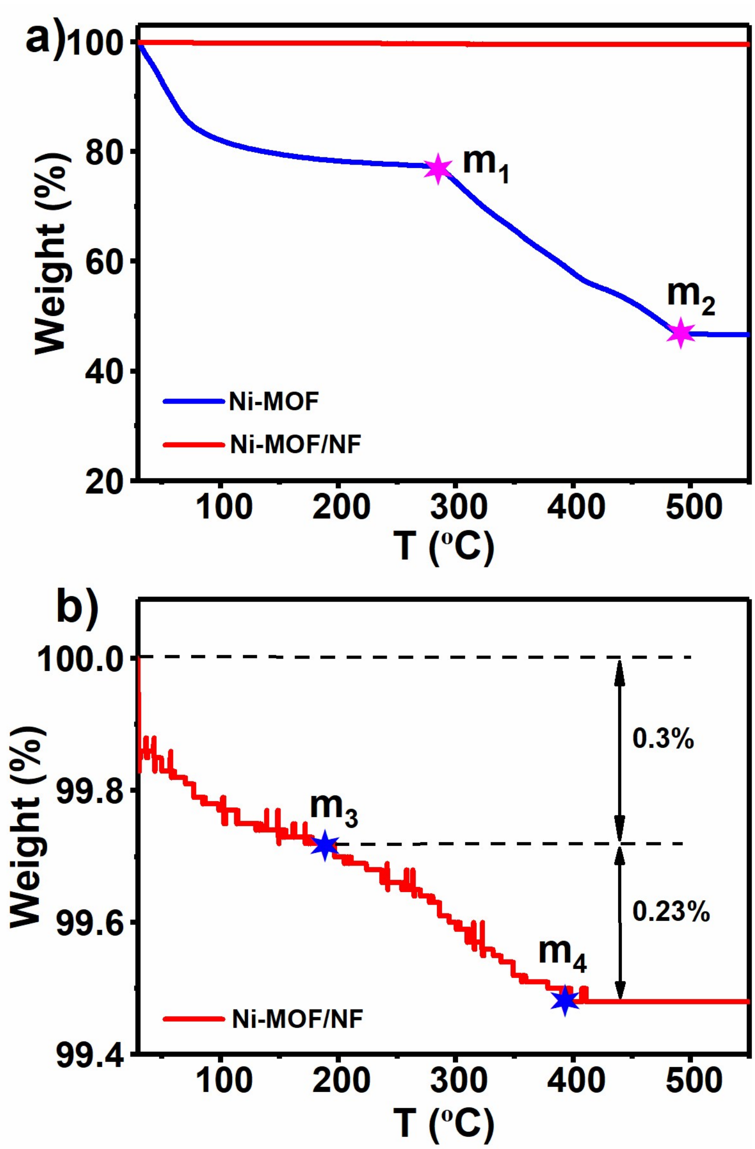

Fig. S6 TGA curve of the Ni-MOF and Ni-MOF/NF (a) and a larger view of Ni-MOF/NF (b).

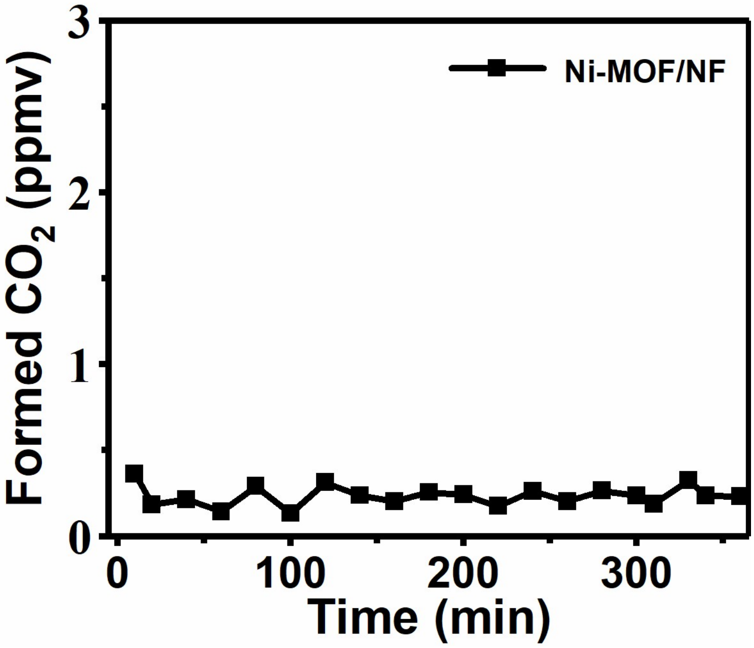

Fig. S7 Evolution of formed CO_2 by Ni-MOF/NF under the investigated photocatalytic oxidation conditions without ethyl acetate. Reaction conditions: a piece of Ni-MOF/NF, air at a flow rate of 35 mL min^{-1}, visible light irradiation.

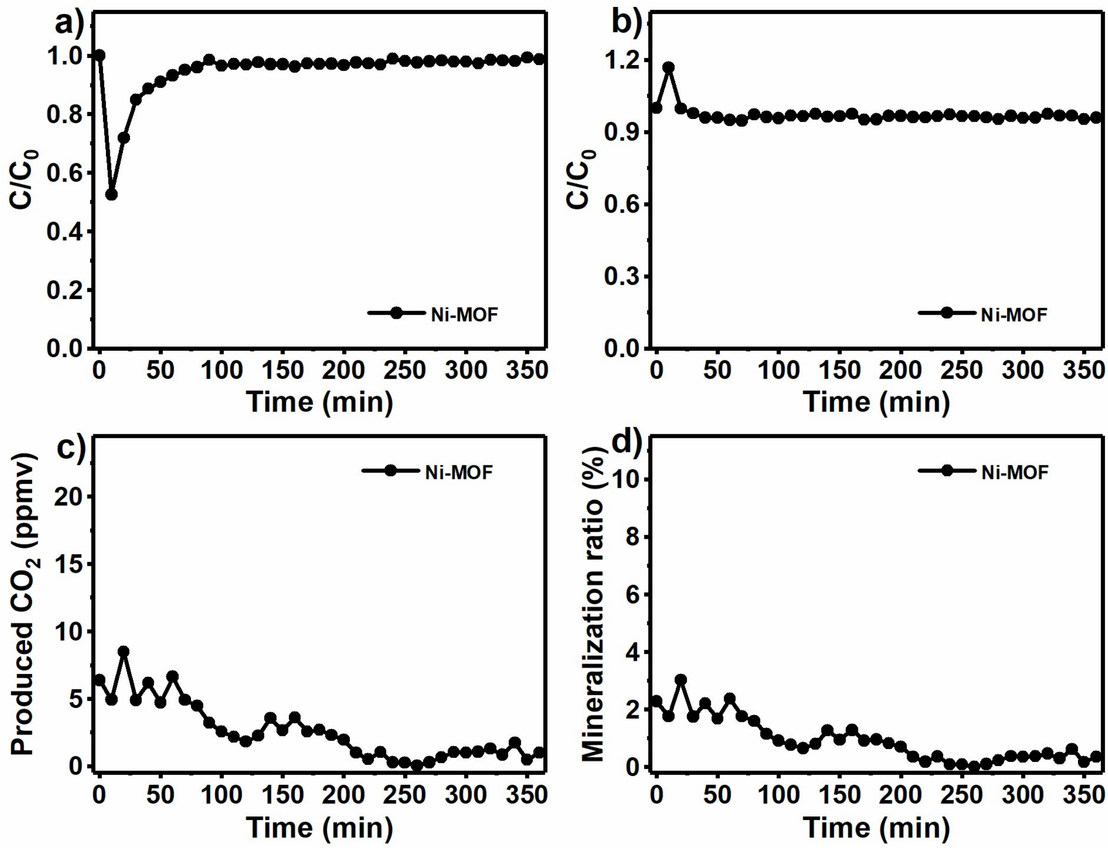

Fig. S8 Adsorption kinetic curves of ethyl acetate by the powder Ni-MOF (a). Evolution of ethyl acetate (b), formed CO_2 (c) and mineralization efficiency (d) during the photocatalytic oxidation of ethyl acetate by Ni-MOF.

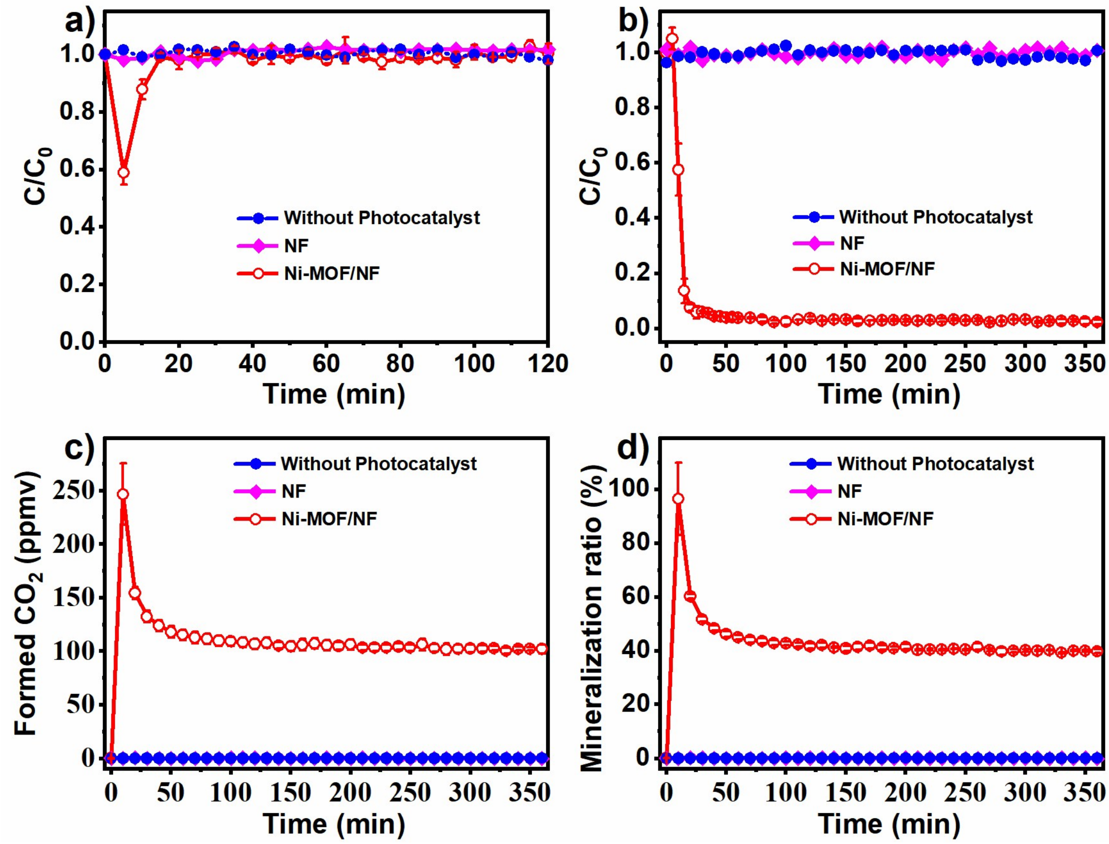

Fig. S9 Adsorption kinetic curves of n-butanol by the Ni-MOF/NF, NF and sample without photocatalyst (a). Evolution of n-butanol (b), formed CO_2 (c) and mineralization ratio (d) during the photocatalytic oxidation by Ni-MOF/NF, NF and sample without photocatalyst.

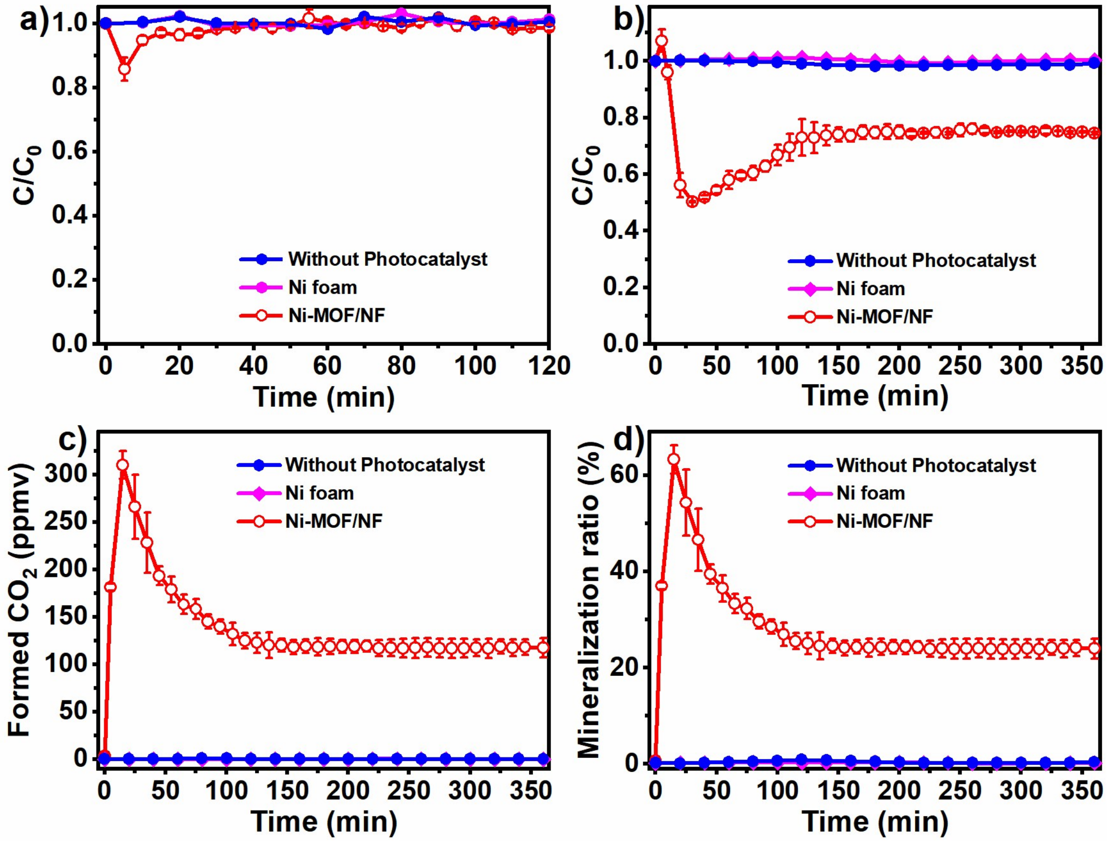

Fig. S10 Adsorption kinetic curves of toluene by the Ni-MOF/NF, Ni foam and without photocatalyst (a). Evolution of toluene (b), formed CO_2 (c) and mineralization efficiency (d) during the photocatalytic oxidation by Ni-MOF/NF, Ni foam and without photocatalyst.

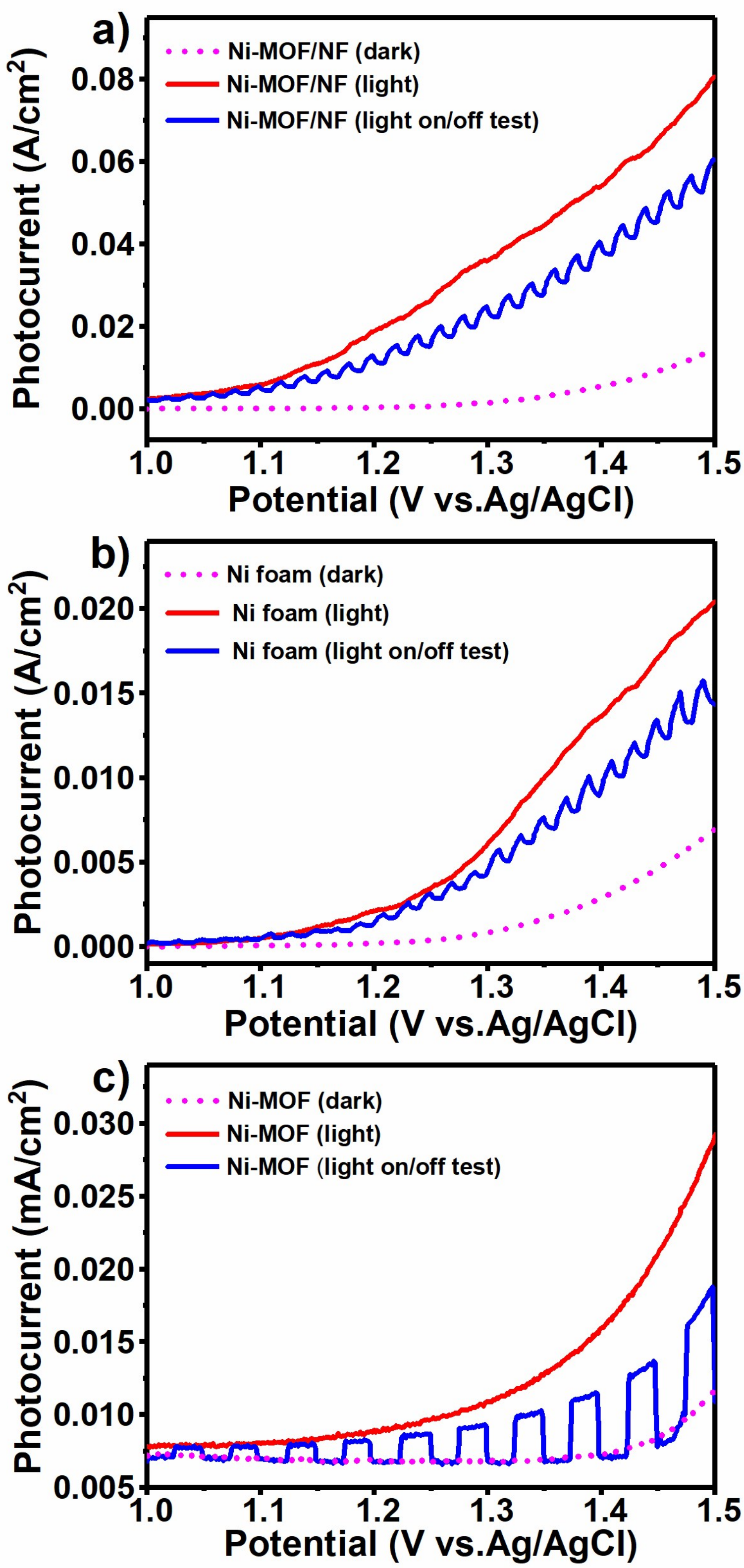

Fig. S11 Photocurrent responses tested by Linear sweep voltammetry (LSV) curve of Ni-MOF/NF (a), Ni foam (b) and Ni-MOF (c) under dark, light and light on/off conditions.

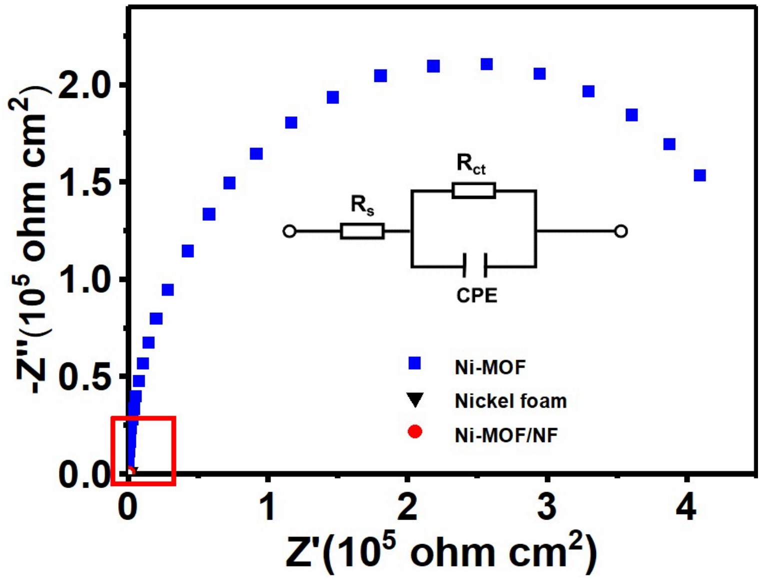

Fig. S12 The equivalent electrical circuit for analysis of EIS spectra.

R_s is the resistance of the solution, R_{ct} is the resistance to electron transfer, and CPE represents the constant phase element.

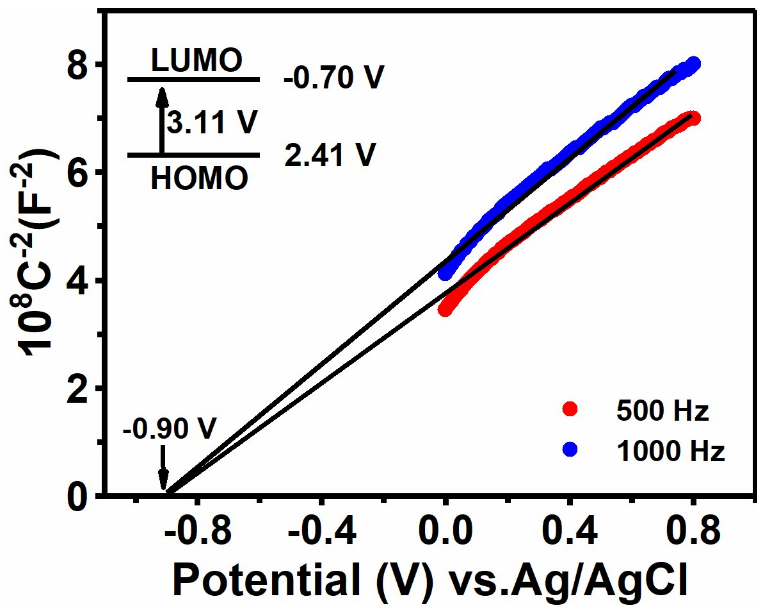

Fig. S13 Mott-Schottky plots for Ni-MOF at frequencies of 500 and 1000 Hz, respectively.

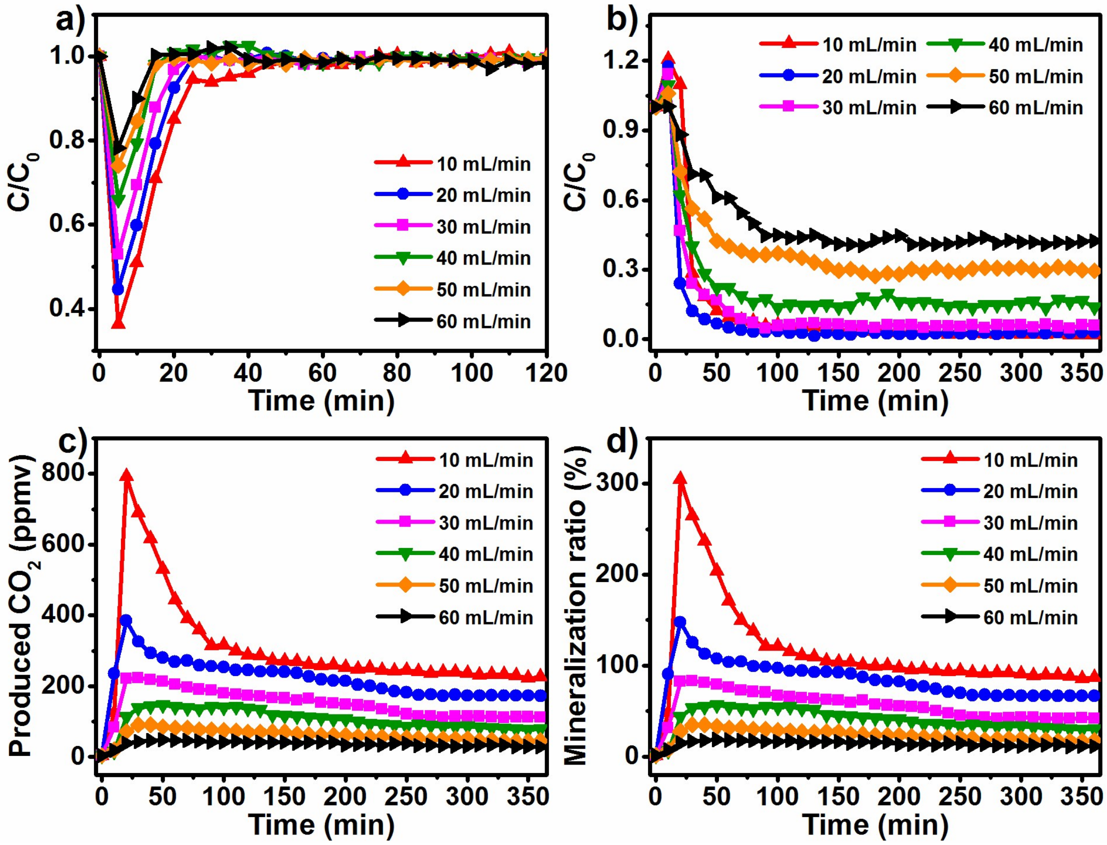

Fig. S14 Adsorption kinetic curves of ethyl acetate by the Ni-MOF/NF(a). Evolution of ethyl acetate (b), formed CO_2 (c) and mineralization efficiencies (d) during the photocatalytic oxidation by Ni-MOF/NF at different flow rates.

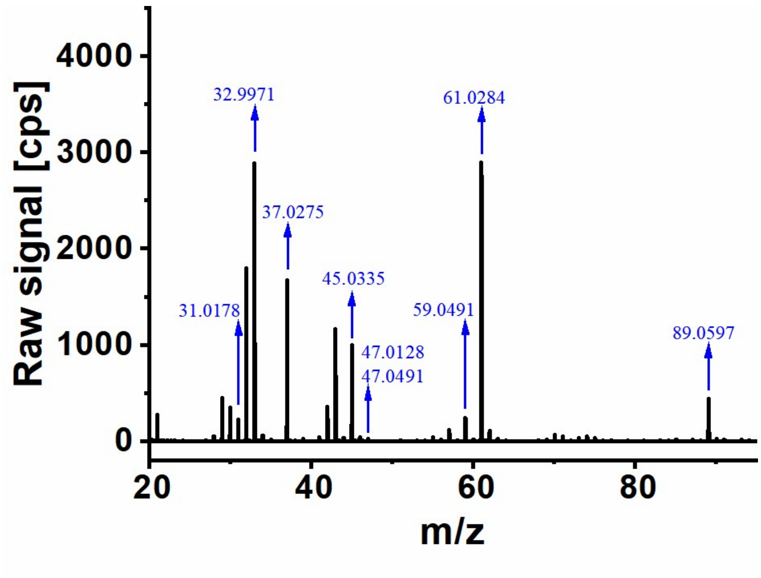

Fig. S15 PTR-TOF-MS spectra for the photocatalytic oxidation of ethyl acetate by Ni-MOF/NF.

Table S1 The specific surface area and porosity of Ni-MOF sample.

Sample	**BET surface area (m^2g^{-1})**	**Total Pore volume (cm^3g^{-1})**	**BJH Pore volume (cm^3g^{-1})**	**BJH pore size (nm)**
Ni-MOF	22.0701	0.058304	0.056697	5.0503

Table S2 Fitting results for equivalent electrical circuits of different samples.

Sample	$R_s(\Omega)$	$R_{ct}(k\Omega)$	CPE(μf)
Ni-MOF/NF	2.79	0.59	0.77
NF	2.11	2.57	0.69
Ni-MOF	19.93	467.03	0.95

Table S3 The photocatalytic performance of ethyl acetate by Ni-MOF/NF in different flow rates within 360 min illumination.

Flow rates	**Removal efficiencies (%)**	**Formed CO_2 (ppmv)**	**CO_2 selectivity (%)**
10	98.1	225.2	88.3
20	97.0	172.6	68.5
30	94.1	111.5	44.2
40	86.2	78.3	34.9
50	70.6	46.0	25.1
60	57.7	28.9	19.2

Table S4 Identified organic compounds by PTR-ToF-MS. [1-4]

Entry	m/z	Name	Formula
1	31.0178	Methanal	CH_2O
2	32.9971		O^{2+}
3	37.0275	Water-cluster	$(H_2O)H_3O^+$
4	45.0335	Acetaldehyde	C_2H_4O
5	47.0128	Formic acid	CH_2O_2
6	47.0491	Ethanol	C_2H_6O
7	59.0491	Propanone	C_3H_6O
8	61.0284	Acetic Acid	$C_2H_4O_2$
9	89.0597	Ethyl Acetate	$C_4H_8O_2$

References

1 H. Wang, S. Chen, Z. Wang, Y. Zhou and Z. Wu, *Appl. Catal. B: Environ.*, 2019, **254**, 339.

2 T. Tsoncheva, A. Mileva, G. Issa, M. Dimitrov, D. Kovacheva, J. Henych, M. Kormunda, N. Scotti, M. Slušná, J. Tolasz and V. Štengl, *J. Environ. Chem. Eng.*, 2018, **6**, 2540.

3 T. Tsoncheva, R. Ivanova, M. Dimitrov, D. Paneva, D. Kovacheva, J. Henych, P. Vomáčka, M. Kormunda, N. Velinov, I. Mitov and V. Štengl, *Appl. Catal. A: Gen.*, 2016, **528**, 24.

4 Y. Yang, Y. Li, Q. Zhang, M. Zeng, S. Wu, L. Lan and X. Zhao, *J. Mater. Chem. A*, 2018, **6**, 14195.